Transport Network Topology as a Determinant of Forced Displacement Dynamics: Case Study of Rail-Based Evacuation from Ukraine

Ivana Malčić[1], Derek Groen[1,2], Valeria Krzhizhanovskaya[1], and Diana Suleimenova[2]

[1] University of Amsterdam, Amsterdam, The Netherlands
[2] Brunel University of London, Uxbridge, United Kingdom
ivana.malcic@student.uva.nl, diana.suleimenova@brunel.ac.uk

Abstract. Conflict-induced displacement is strongly shaped by transportation networks, yet most displacement models represent mobility as continuous or distance-based, neglecting network constraints such as corridor structure, connectivity, and capacity. This limits the ability of existing approaches to capture evacuation dynamics in situations where movement is mediated by infrastructure-specific determinants.
This paper presents an agent-based model of infrastructure-constrained forced displacement that explicitly represents a real-world railway network. Implemented in Flee 3, the model simulates displacement during the early phase of the 2022 Russian invasion of Ukraine by dynamically generating agents in response to conflict-onset data from ACLED and routing movement exclusively along operational rail corridors toward railway-accessible border checkpoints. Simulations cover the period from February to June 2022, producing daily arrival counts at eight major border crossings for validation against a curated empirical dataset.
The model achieves strong overall fit, with a median across-camp average relative difference (ARD) of 0.31 and sustained post-surge errors below 20% for most corridors. Beyond aggregate fit, the results reveal a clear two-phase structural transition. During the initial surge, flows are distributed across multiple corridors, with no single route consistently dominant. In the stabilized phase, flows consolidate sharply, indicating persistent single-corridor dominance. Ultimately, the findings suggest displacement trajectories are not governed by distance or conflict intensity alone, but by network topology, asymmetric capacity constraints, and endogenous corridor competition.

Keywords: forced displacement · agent-based modeling · Ukraine · network-constrained mobility · evacuation dynamics · railway networks · Flee 3

1 Introduction

Conflict-induced displacement is an increasingly prominent feature of global population mobility, referring to the involuntary movement of people escaping armed conflict, political instability, or systematic human rights violations [1]. The 2022

ICCS Camera Ready Version 2026
To cite this paper please use the final published version:
DOI: 10.1007/978-3-032-29915-4_4

invasion of Ukraine triggered one of the most rapid and large-scale displacement events in modern history, with millions fleeing their homes and crossing into neighboring countries.

Unlike voluntary migration, conflict-induced displacement is characterized by sudden onset, limited individual choice, and strong dependence on infrastructure, humanitarian responses, and institutional actions. These conditions pose challenges for quantitative modeling, particularly during early phases when movements are rapid, unpredictable, and uncoordinated. In large-scale evacuations, infrastructure is not merely a passive medium; it actively structures mobility by enabling, constraining, and redirecting flows. Likewise, transport modes play distinct roles in this process: rail systems operate along fixed corridors and enable coordinated high-capacity movement, while road-based transport tends to be more decentralized and allows adaptive routing. Despite these differences, relatively little modeling work explicitly accounts for transport modality in displacement dynamics.

To fill this gap, the present paper investigates the role of railway networks in shaping large-scale forced displacement, using the 2022 Russian invasion of Ukraine as a case study. To this end, an agent-based model is developed using Flee 3 [2], embedding an operational railway network and coupling it with conflict-onset dynamics and population distributions. Displaced individuals are represented as agents moving from conflict-affected areas to border checkpoints along realistic rail corridors. The simulation covers the early phase of the invasion (February 22 to June 22, 2022) and generates daily arrival counts at major border crossings, which are validated against observed data.

Overall, this work investigates how explicitly modeling railway infrastructure alters our understanding of forced displacement during conflict. In particular, it assesses whether network-constrained evacuation dynamics can reproduce observed refugee flows and reveal structural consolidation effects. By analyzing corridor hierarchy, flow concentration, and the emergence of dominant routes, we show how network topology actively governs displacement trajectories.

2 Related Work

Agent-based models (ABMs) are widely used to simulate forced displacement in contexts such as natural disasters and armed conflict. Early models largely relied on distance-driven mobility assumptions, with individuals moving toward safety along the shortest paths. More recent approaches incorporate greater behavioral heterogeneity and social interactions, enabled by increased computational capacity [3, 4].

Insights from transport geography show that physical constraints such as topography, node-link structures, and grade limitations shape land transport networks, imposing a natural convergence of routes that create a certain degree of centrality [5]. These properties are particularly pronounced in railway systems, which operate along fixed corridors and impose limited routing flexibility alongside station-level bottlenecks. Such structural characteristics are not

ICCS Camera Ready Version 2026
To cite this paper please use the final published version:
DOI: 10.1007/978-3-032-29915-4_4

fully represented in mode-agnostic displacement models. The use of rail transport for medical evacuations, cross-border displacement, and logistic support has been directly observed during the ongoing conflict in Ukraine, where the railway network has proven to be indispensable for large-scale evacuation efforts [6]. Empirical studies further document their use in large-scale medical evacuation and humanitarian operations [7].

Recent work by Mehrab et al. [3, 8] examines forced displacement dynamics in Ukraine using agent-based approaches that capture adaptive decision-making under crisis conditions and explore the impact of environmental and social factors on displacement trajectories. Beyond displacement modeling, large-scale agent-based transportation frameworks have been developed to analyze evacuation dynamics in road-based contexts. Wolshon et al. [9] applied the TRANSIMS microscopic framework to study megaregional hurricane evacuations. Similarly, MATSim (Multi-Agent Transport Simulation) [10] provides a large-scale agent-based platform widely used for urban and regional transport analysis.

Despite these advances, a key limitation across displacement and transport modeling approaches is the lack of integration between conflict-driven migration dynamics and infrastructure-explicit mobility constraints. Some displacement models [3, 8] incorporate behavioral and spatial processes but typically do not constrain movement using transport infrastructure, while transport frameworks such as TRANSIMS and MATSim explicitly represent transport network topology but are not equipped to capture conflict-induced displacement. This abstraction may ultimately lead to miss-estimation of corridor-level flows and higher uncertainty in route allocation. In contrast, the present study addresses this gap by integrating infrastructure-constrained mobility with conflict-driven displacement dynamics in a unified modeling framework to examine how these processes jointly shape displacement patterns.

3 Methodology

Agent-based modeling (ABM) provides a suitable framework for this study as it allows the simultaneous representation of network-level physical constraints together with individual-level behavioral drivers. By explicitly modeling heterogeneous agents, ABMs can reproduce evacuation dynamics including queue formation at stations, congestion spillovers to secondary checkpoints, and route rerouting under capacity pressure [11].

3.1 Modeling Framework

Flee is an agent-based modeling framework designed to simulate conflict-driven displacement under crisis conditions, with explicit representation of movement processes and destination constraints [2, 12].

Agent Decision-Making and Movement Rules In Flee, displacement is modeled as a two-stage process consisting of conflict-driven agent generation

ICCS Camera Ready Version 2026
To cite this paper please use the final published version:
DOI: 10.1007/978-3-032-29915-4_4

and network-constrained movement. Generation of agents at conflict zones is triggered dynamically following conflict onset: once a conflict-zone node becomes active, a fraction of the local population representing civilians initiating displacement is released into the network.

At each discrete time step, agents first decide whether to move according to probabilistic decision rules depending on their current location type; agents in conflict zones move with probability `conflict_movechance`, whereas agents in transit locations move with `default_movechance`. Those in camps stay there, representing people who crossed the border.

If an agent decides to move, it evaluates a set of reachable destinations determined by `awareness_level`. In Flee, route choice is based on weighted routing, combining distance decay, destination attractiveness, and capacity constraints. For our model, this can be summarized as

$$A_j \propto \frac{w_j}{d_{ij}^{\alpha}} \cdot C_j,$$

where d_{ij} denotes the network distance from the current location i to destination j, α is given by `distance_power`, w_j represents destination attractiveness, primarily determined by `camp_weight`, and C_j captures capacity effects which reduce attractiveness as occupancy approaches capacity, controlled by `capacity_scaling`.

Agents then probabilistically select a destination based on the normalized attractiveness score and proceed following a planned route toward it. Movement is executed incrementally along the network, with daily travel distances bounded by `max_move_speed`. Movement is strictly constrained to the underlying railway network: agents can only traverse predefined links between nodes, and no off-network routing is permitted.

Node Creation: Camps, Conflict Zones and Towns The railway network was represented as a set of discrete locations connected by passenger rail links, with nodes grouped into three Flee-native categories: conflict zones, towns, and camps, as described in Table 1. To reduce complexity while preserving national connectivity, one representative train station was selected per oblast. Camps were defined at major railway-accessible border crossings shown in Table 2. Conflict onset dates for each conflict-zone node were assigned using data from the Armed Conflict Location and Event Data Project (ACLED) [13]. The simulation covers the period from February 22, 2022 to June 22, 2022 (120 days), while the initial populations at each node were estimated using aggregated demographic data reported at the oblast level. The full list of modeled locations with their associated attributes is available in the supplementary repository [14].

Railway Network Construction Figure 1 shows the full set of modeled nodes and links used in the simulation, including conflict zones, towns, and border camps, corresponding to the three principal evacuation corridors described below.

ICCS Camera Ready Version 2026
To cite this paper please use the final published version:
DOI: 10.1007/978-3-032-29915-4_4

Table 1. Classification and attributes of model locations.

Category	Description	Key attributes
Conflict zones	Major railway stations located in or near active conflict areas during the simulation period, serving as primary departure points for displaced agents.	Geographic coordinates; administrative region; location type; population; conflict start date.
Camps	Railway-accessible border checkpoints functioning as final safe destinations. Agent movement terminates upon arrival. Each camp is assigned a `camp_weight` reflecting relative reception capacity.	Geographic coordinates; administrative region; location type; capacity; camp weighting factor.
Towns	Intermediate stations located in areas unaffected by conflict. These nodes facilitate network connectivity but do not directly generate displacement.	Geographic coordinates; administrative region; location type; population.

Table 2. Border camps grouped by destination country.

Destination country	Camps / border checkpoints
Poland	Mostyska–Przemyśl; Yahodyn–Dorohusk; Volodymyr-Volynskyi–Hrubieszów
Hungary	Chop (Druzhba)–Záhony
Slovakia	Mukachevo–Košice
Moldova	Reni–Giurgiulești; Mohyliv-Podilskyi–Volchinets
Romania	Vadul–Siret–Vicșani

The network was constructed by identifying major rail corridors across the country and compiling inter-regional links from open railway data and verified schedules. Realistic distances (km) were assigned using geodesic estimates along railway alignments to preserve plausible travel times and network scale. The final topology reflects three principal corridors:
East-West long-haul routes connecting major eastern centers to western regions (e.g., Kharkiv-Kyiv; Dnipro-Kropyvnytskyi-Vinnytsia-Lviv).
South-West transit corridors linking coastal cities to border checkpoints via Odesa (e.g., Kherson-Mykolaiv-Odesa-Reni).
Western border approaches enabling cross-border movement into Poland, Slovakia, and Hungary (e.g., Lviv-Mostyska; Mukachevo-Košice; Uzhhorod-Chop).

3.2 Assumptions, Parameters and Model Validation

The simulation relied on selected parameters in `simsetting.yml`, chosen to reflect evacuation conditions listed in Table 3.

ICCS Camera Ready Version 2026
To cite this paper please use the final published version:
DOI: 10.1007/978-3-032-29915-4_4

Fig. 1. Map of Ukraine with red nodes representing train stations (conflict zones), yellow nodes representing towns, and green nodes representing border checkpoints (camps). The base map is derived from OpenStreetMap and used under the Open Database License (ODbL).

Location Capacities In Flee, each location is associated with a population or capacity parameter that constrains how many agents can be generated from, or absorbed by, that node over time. For conflict-zone nodes, the population parameter represents the pre-war civilian population, determining the upper bound on the total number of agents that can be generated, or displaced, from each location. For camp nodes, the capacity parameter represents an aggregate approximation of the maximum number of arrivals that can be accommodated over the simulation period. Capacity assignments reflect the relative scale of border infrastructure, staffing, and onward transport options, informed by host-country context and qualitative reports from the early phase of the conflict. Major railway crossings were therefore assigned substantially higher capacities than smaller or less-connected checkpoints.

Camp Weights In addition to absolute capacity limits, Flee allows destination attractiveness to be modulated through the `camp_weight` parameter, biasing movement probabilities towards more desired camps. This separation enables the model to distinguish between where agents preferentially travel from how many arrivals a location can ultimately absorb. In this model, camp weights were assigned on a relative scale to reflect differences in attractiveness within the same border region. Weighting factors account for arbitrary differences in connectivity to onward transport networks, perceived economic opportunity, and host-country's institutional capacity; for example, the Mostyska–Przemyśl crossing is assigned a higher value than Volodymyr-Volynskyi–Hrubieszów crossing, reflecting its stronger rail connectivity and higher observed throughput.

ICCS Camera Ready Version 2026
To cite this paper please use the final published version:
DOI: 10.1007/978-3-032-29915-4_4

Table 3. Key simulation parameters and rationale.

Parameter	Bounds	Value	Description and rationale
`max_move_speed`	$[0, \infty)$	700.0	Maximum daily travel distance (km), reflecting intercity rail transport capacity.
`max_walk_speed`	$[0, \infty)$	35.0	Maximum daily walking distance (km), representing short access segments to stations or camps.
`awareness_level`	$[1, 3]$	3	Agents evaluate destinations up to three network links away, approximating route planning based on available connections and information.
`distance_power`	$[0, 1]$	0.7	Controls the influence of distance on destination choice, biasing agents toward shorter routes while allowing other factors to influence decisions.
`conflict_movechance`	$[0, 1]$	1.0	Daily probability of leaving conflict zones. A value of 1.0 ensures immediate displacement upon conflict exposure.
`default_movechance`	$[0, 1]$	0.4	Baseline daily movement probability outside conflict zones, capturing gradual and anticipatory displacement dynamics.
`capacity_scaling`	$[0, 1]$	0.8	Controls how rapidly destination attractiveness decreases as capacity is approached, representing congestion and administrative constraints.

Validation Data Construction In absence of an external curated rail crossing dataset, a custom validation dataset was constructed by combining multiple country-specific border statistics with additional rail-use evidence and cross-checking the result against an aggregate benchmark.

1. **Border crossing data analysis.** Daily counts of border crossings were collected for each neighboring country over the period February–June 2022 using official national statistics and reports [15–19].
2. **Estimation of train use.** Because border statistics do not report transport mode, the proportion of refugees traveling by train was estimated using two credible independent survey-based assessments conducted in Poland and Slovakia during mid-March 2022. Both surveys report that approximately 18% of respondents entering Poland and Slovakia used rail transport [20, 21]. For modeling purposes, this value was rounded to 20% to account for uncertainty in survey-based estimates.
3. **Camp-level cross-validation.** Estimated rail-based arrivals per country were further disaggregated to individual border checkpoints (camps) and cross-checked against additional qualitative and quantitative sources, includ-

ICCS Camera Ready Version 2026
To cite this paper please use the final published version:
DOI: 10.1007/978-3-032-29915-4_4

ing reports on railway operations, humanitarian logistics, and observed congestion at specific crossings.

4. **Aggregate plausibility check.** To assess overall consistency, daily rail-based arrival estimates were aggregated over the full simulation period, yielding a total of 1,380,232 individuals. This figure was compared against an independent benchmark of roughly 1.3 million derived from total registered refugees by June 2022 multiplied by the assumed 20% rail share. The agreement between these values (within 5%) provides a robust plausibility check for the constructed dataset.

To operationalize the data, the estimated rail share was applied to daily country-level border crossing totals and then distributed across multiple railway-accessible checkpoints according to observed usage patterns informed by reported train frequencies, infrastructure capacity, and qualitative accounts of evacuation flows from media reports.

3.3 Evaluation Metrics

To assess how rail-based evacuation patterns consolidate into dominant routes over time, two complementary dimensions were evaluated: (i) structural concentration of flows across corridors and (ii) model–validation data agreement at the camp level. Interpretive guidance for the concentration measures and the ARD metric is provided in the Supplementary Information (Appendix B).

Corridor Concentration Metrics Rail-based displacement does not distribute uniformly across all border crossings, as flows may be directed to a limited number of high-capacity corridors. To quantify this hierarchical organization, daily camp-bound arrivals were aggregated by destination country. Let $F_i(t)$ denote total arrivals to corridor i on day t, and define corridor shares as

$$s_i(t) = \frac{F_i(t)}{\sum_j F_j(t)}. \tag{1}$$

Because $\sum_i s_i(t) = 1$, concentration measures reflect structural distribution independently of total evacuation volume. Three complementary metrics were computed.

Concentration Ratio (CR1). The concentration ratio, here interpreted as the dominance index,

$$H(t) = \max_i s_i(t) \tag{2}$$

captures the share of displaced people absorbed by the single largest corridor. This measure directly quantifies whether evacuation is governed by one structurally dominant route.

ICCS Camera Ready Version 2026
To cite this paper please use the final published version:
DOI: 10.1007/978-3-032-29915-4_4

Herfindahl–Hirschman Index (HHI). The HHI,

$$HHI(t) = \sum_i s_i(t)^2, \tag{3}$$

measures overall concentration across all corridors. Unlike CR1, which isolates only the largest share, HHI captures the cumulative contribution of secondary corridors.

Gini Coefficient. The Gini coefficient measures inequality across $\{s_i(t)\}$, capturing disparity between dominant and marginal corridors and therefore emphasizing relative imbalance in the full distribution.

These three metrics distinguish between (i) single-corridor dominance, (ii) system-wide concentration, and (iii) inequality across competing routes, and are together used to analyze emergent corridor hierarchy.

Error Metric (ARD) Model–validation data agreement was evaluated using the Average Relative Difference (ARD), following prior Flee validation practice [22].

Let $S_k(t)$ denote simulated arrivals and $D_k(t)$ observed arrivals at camp k on day t, then the daily ARD is defined as

$$E(t) = \frac{\sum_k |S_k(t) - D_k(t)|}{\sum_k D_k(t)}. \tag{4}$$

This formulation aggregates absolute deviations across camps and normalizes by total observed arrivals, yielding a dimensionless measure of proportional system-level mismatch. ARD values are context-dependent, and as such need to be interpreted with regards to the specific application; a useful reference range can be obtained via prior studies using Flee which reported acceptable ARD values on the order of 0.2–0.4 [22].

4 Results

4.1 Camp-level Model Fit

The model error exhibits a clear temporal structure. During the initial phase (approximately days 1–20), daily relative errors are elevated across most corridors. After this transient adjustment period, errors decline substantially and remain low for the remainder of the simulation. From early May onward, median daily ARD across camps remains below 0.2, as seen in Figure 2, indicating stable alignment once displacement flows settle.

Error dynamics also vary systematically across corridors. From Figure 3, it is visible that high-throughput evacuation corridors such as Mostyska–Przemyśl and Vadul–Siret–Vicșani exhibit comparatively balanced and stable error patterns after the early surge. In contrast, peripheral camps, including Mohyliv–Volchinets and Reni–Giurgiulești, display greater temporal volatility.

ICCS Camera Ready Version 2026
To cite this paper please use the final published version:
DOI: 10.1007/978-3-032-29915-4_4

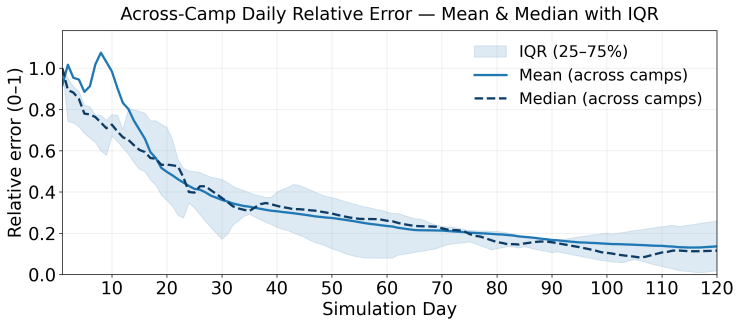

Fig. 2. Across-camp ARD showing mean, median, and inter-quartile range of daily errors between simulated and observed arrivals.

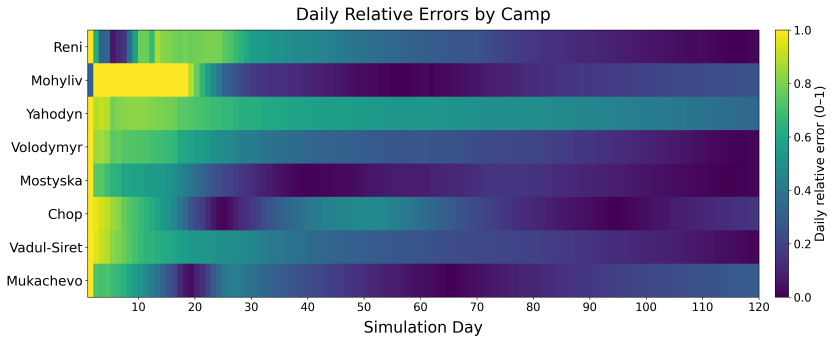

Fig. 3. Heatmap of daily relative errors for each simulated border checkpoint (camp) over the 120-day simulation period (ARD camp-specific components). Camp names are abbreviated for compactness; full names can be found in Table 2

Cumulative arrivals in Figure 4 confirm these patterns. High-throughput corridors such as Mostyska–Przemyśl and Vadul–Siret–Vicșani track observed data closely over most of the simulation, whereas peripheral lower-volume corridors show larger early deviations and slower convergence.

High-throughput corridors The strongest and most consistent agreement is observed along major evacuation routes. Mostyska–Przemyśl exhibits the lowest mean and median ARD (0.169 and 0.095), indicating sustained alignment across the full simulation horizon. Vadul–Siret–Vicșani shows similarly stable behavior, with moderate median (0.259) and limited variability relative to peripheral routes. For these corridors, discrepancies are largely confined to the early surge period.

Intermediate corridors Mukachevo–Košice (median ARD 0.203), Chop (Druzhba)–Záhony (median 0.204), and Volodymyr-Volynskyi–Hrubieszów (median 0.269)

ICCS Camera Ready Version 2026
To cite this paper please use the final published version:
DOI: 10.1007/978-3-032-29915-4_4

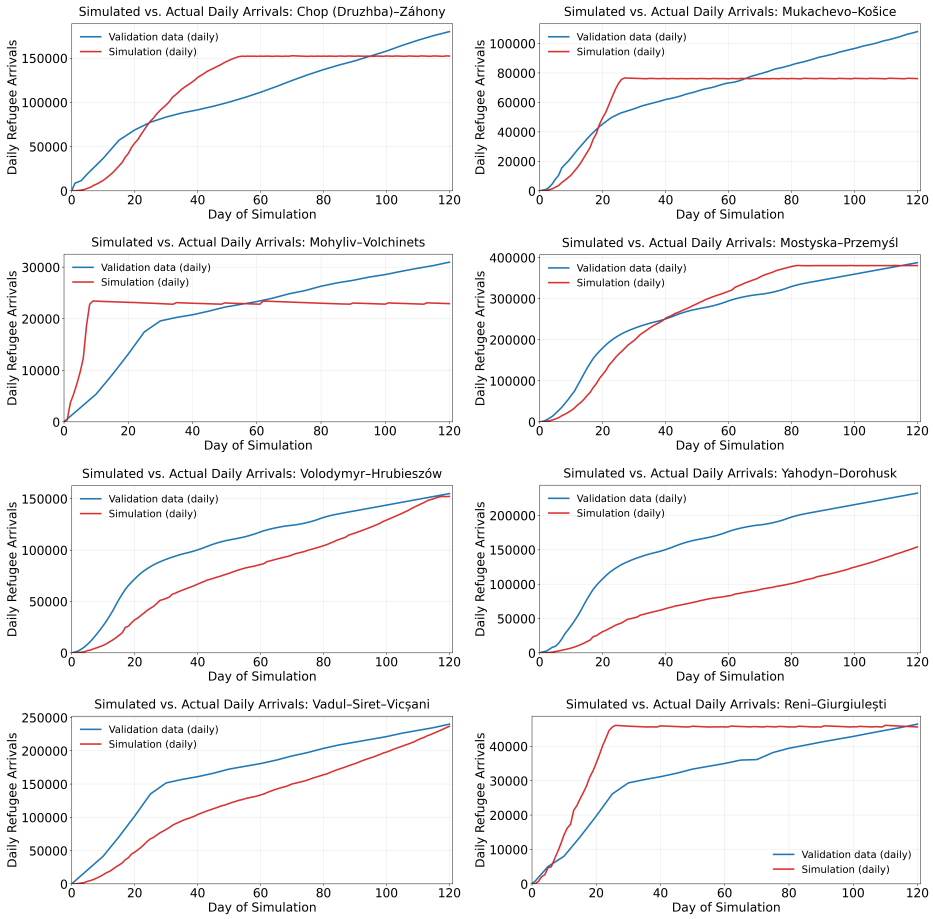

Fig. 4. Simulated versus observed cumulative daily refugee arrivals for each border camp over the 120-day simulation period.

display low error and low variability, with means and medians following closely together. These corridors show stable but less precise alignment compared to the highest-volume routes.

Peripheral / low-volume corridors Greater variability is observed in lower-volume routes. Yahodyn–Dorohusk shows persistently elevated deviation, with the highest mean and median ARD (0.555 and 0.530), reflecting sustained under-prediction. Mohyliv-Podilskyi–Volchinets is characterized by pronounced variability rather than systematic bias, with the largest maximum error (4.313) but a substantially lower median (0.165), indicating occasional but extreme deviations. Reni–Giurgiulești (median ARD 0.283) exhibits a similar early overshoot

ICCS Camera Ready Version 2026
To cite this paper please use the final published version:
DOI: 10.1007/978-3-032-29915-4_4

followed by slower growth. Across these peripheral corridors discrepancies extend beyond the initial shock phase and are more temporally volatile.

Full descriptive statistics of the daily ARD time series for each camp are provided in Supplementary Table S1 (see Supplementary Appendix C).

4.2 Corridor Hierarchy

During the early phase (days 1–14), evacuation flows are distributed. The mean dominance index is $H = 0.485$, indicating that the largest corridor captures less than half of daily camp-bound flow on a typical day. Early-phase corridor shares are relatively balanced: Poland (mean share 0.363) and Moldova (0.325) both function as major channels, while Romania, Hungary, and Slovakia retain consistent secondary participation. By contrast, in the stabilized phase (days 30–120), flows consolidate sharply. Mean dominance increases to 0.634, and concentration metrics rise substantially (Gini: 0.373 → 0.619; HHI: 0.352 → 0.507), reflecting a transition toward persistent single-corridor dominance. Poland-bound routes capture an average share of 0.634 and are dominant on 98.9% of stabilized-phase days, while Romania emerges as a stable secondary corridor (mean share 0.275). Other corridors become marginal. The full distribution of daily dominance values $H(t)$ is reported in Supplementary Appendix C, Table S2.

Table 4. Corridor concentration metrics by phase.

Phase	Mean H	Mean Gini	Mean HHI
Early (1–14)	0.485	0.373	0.352
Stabilized (30–120)	0.634	0.619	0.507

Per-corridor metrics further reinforce this structural shift. In the early phase, Poland is dominant on 64.3% of days, but Moldova also exhibits substantial activity (active on 100% of days). In the stabilized phase, however, dominance becomes nearly exclusive: Poland accounts for almost all dominant days, while Hungary, Moldova, and Slovakia display reduced activation frequency and low share variability. Share standard deviations decline for dominant corridors, indicating increased temporal stability. Activation timing further highlights the rapid onset of corridor competition: all major corridors exceed their activation thresholds within the first two days of the simulation, confirming that hierarchy does not emerge from delayed availability. Comprehensive dominance distributions, activation thresholds, and per-corridor structural statistics for both phases are reported in Supplementary Tables S2–S5 (Supplementary Appendix C).

4.3 Model Performance and Comparison

To contextualize model performance, the results are also compared with prior work on forced displacement and existing Flee-based studies. At the aggregate

ICCS Camera Ready Version 2026
To cite this paper please use the final published version:
DOI: 10.1007/978-3-032-29915-4_4

level, we compare our results to the Ukraine-specific Network Agency model [3]. Mehrab et al. report a root mean squared percentage error (RMSPE) of 0.24 and a Pearson correlation coefficient (PCC) of 0.98 for aggregate daily outflows, whereas the present model yields an RMSPE of 0.27 and a PCC of 0.993. This indicates similar accuracy even without explicit social influence mechanisms, and using a purely rail-constrained network, thus supporting the finding that infrastructure topology is a first-order determinant of displacement patterns. Metric-level comparison below the aggregate level, however, is not possible because Mehrab et al. do not report corridor-level or camp-level error distributions, and their model does not disaggregate by transport mode.

The results can also be interpreted in the context of prior Flee validation studies. Existing work shows that model performance improves as additional information on routing, destination attractiveness, and capacity constraints is incorporated. In particular, Suleimenova and Groen [22] report consistently higher ARD values for simpler configurations, suggesting that reduced formulations (e.g., distance-only or fixed-attractiveness assumptions) would yield weaker agreement with observed data. The median across-camp ARD value of 0.31 obtained in our model lies within the range reported across historical Flee applications [2] and compares favorably with crisis-specific studies such as the Tigray case [23]. This is notable given the structural complexity of the present case, which combines a large transport network, a high-speed mobility regime, and a custom validation dataset.

5 Discussion

The results indicate that rail-based displacement dynamics exhibits a two-phase structure: an early surge regime followed by structural consolidation. The early phase reflects not only empirical volatility but also an initialization effect of the modeling framework.

In the first weeks, flows are distributed across multiple corridors, routing patterns fluctuate, and model–data error peaks. This arises from two interacting mechanisms. First, real-world displacement is inherently unstable immediately after escalation, with uncertainty, congestion spillovers, and rapid rerouting. Second, the model undergoes a transient "warm-up": at $t = 0$ camps are empty and therefore highly attractive, while capacity constraints have not yet taken effect. As agents accumulate at border nodes, capacity scaling progressively reshapes destination probabilities, amplifying early routing differences and increasing ARD. Incorporating time-dependent movement behavior or improved initialization in future work may therefore reduce early-phase discrepancies.

From approximately the first month onward, the system enters a more stable regime. Flows consolidate onto high-capacity corridors, peripheral crossings become episodic, and ARD remains low. This structural consolidation is further reflected in the emergence of a clear corridor hierarchy. High-capacity routes consistently dominate system-level flows, while secondary corridors remain active

ICCS Camera Ready Version 2026
To cite this paper please use the final published version:
DOI: 10.1007/978-3-032-29915-4_4

but contribute marginally, indicating that displacement becomes increasingly governed by network topology and capacity asymmetries over time.

The validation results place the model in the context of prior work: aggregate-level accuracy is similar to that reported in recent Ukraine-specific modeling, while camp-level ARD values fall within the range observed across historical Flee applications. The present model, however, additionally resolves corridor-level structure, allowing explicit examination of route hierarchy.

Several limitations remain. Movement parameters were calibrated heuristically rather than estimated from independent data, and assumptions such as fixed rail use and static capacities significantly simplify time-varying operational conditions. Moreover, the simplification of the rail network to one station per oblast may omit important local feeder dynamics that could influence route choice and the timing of arrivals.

Nonetheless, the framework is structurally transferable. It relies on three core elements—transport network topology, conflict-driven agent generation, and capacity-driven destination attractiveness—which can be adapted to other contexts given appropriate data. In particular, the network representation can be extended to multimodal systems, while conflict and population inputs can be derived from region-specific datasets, although the relative importance of infrastructure constraints may vary across settings, particularly where transport networks are less centralized.

The distinction between surge and stabilization phases also has practical implications. During the early phase, flexibility is critical: temporarily expanding throughput across multiple crossings and rapidly reallocating transport capacity can help mitigate congestion and spillovers. In the later phase, system performance depends on the reliability of dominant corridors, as disruptions at major hubs are likely to propagate across the network. Maintaining capacity at high-throughput crossings, while preserving secondary routes as contingency options, is therefore key.

Supplementary Information and Code Availability: Supplementary Information, as well as the input information, output results and figures as well as code can be found at [14].

References

1. Sironi, A., Bauloz, C. and Emmanuel, M. (eds.) (2019) *Glossary on Migration*, International Migration Law, No. 34, International Organization for Migration, Geneva.
2. Ghorbani, M. et al. (2024) *Flee 3: Flexible agent-based simulation for forced migration*, Journal of Computational Science, 81, p. 102371.
3. Mehrab, Z., Stundal, L., Swarup, S., Venkatramanan, S., Lewis, B., Mortveit, H. and Colwell, R. R. (2024) *Network Agency: An Agent-based Model of Forced Migration from Ukraine*, Proceedings of the 23rd International Conference on Autonomous Agents and Multiagent Systems (AAMAS), pp. 1372–1380.

ICCS Camera Ready Version 2026
To cite this paper please use the final published version:
DOI: 10.1007/978-3-032-29915-4_4

4. Pan, X., Han, C. S., Dauber, K. and Law, K. H. (2007) *A multi-agent based framework for the simulation of human and social behaviors during emergency evacuations*, AI & Society, 22(2), pp. 113–132.
5. Rodrigue, J.-P., Comtois, C. and Slack, B. (2016) *The Geography of Transport Systems*, 4th ed., Routledge, New York.
6. The European Correspondent (2024) *Freedom travels by train*. Available at: https://europeancorrespondent.com/en/r/freedom-travels-by-train (Accessed: 9 August 2025).
7. Walravens, S. et al. (2023) *Characteristics of Medical Evacuation by Train in Ukraine, 2022*, JAMA Network Open, 6(6), e2319726.
8. Mehrab, Z. et al. (2024) *An agent-based framework to study forced migration: A case study of Ukraine*, PNAS Nexus, 3(3), p. pgae080.
9. Wolshon, B. et al. (2015) *Agent-Based Modeling for Evacuation Traffic Analysis in Megaregion Road Networks*, Procedia Computer Science, 52, pp. 908–913.
10. Horni, A., Nagel, K. and Axhausen, K. W. (eds.) (2016) *The Multi-Agent Transport Simulation MATSim*, Ubiquity Press.
11. Xu, Z., Bai, Q., Shao, Y., Hu, A. and Dong, Z. (2022) *A review on passenger emergency evacuation from multimodal transportation hubs*, Journal of Traffic and Transportation Engineering (English Edition), 9(4), pp. 571–590.
12. Groen, D., Suleimenova, D. and Bell, D. (2023) *Flee Documentation*. Available at: https://flee.readthedocs.io/en/master/ (Accessed: 9 August 2025).
13. Armed Conflict Location and Event Data Project (ACLED) (2025) *Ukraine Conflict Event Data*. Available at: https://acleddata.com/ (Accessed: 9 August 2025).
14. Malcic, I. (2026) *Supplementary Information: Transport Network Topology as a Determinant of Forced Displacement Dynamics: Case Study of Rail-Based Evacuation from Ukraine*. Available at: https://doi.org/10.5281/zenodo.18762088
15. Urbán, F. (2023) *Characteristics of Migration from Ukraine to Hungary in the Last Decade*, Hungarian Law Enforcement, 1, pp. 205–217.
16. Duszczyk, M. and Kaczmarczyk, P. (2022) *The War in Ukraine and Migration to Poland: Outlook and Challenges*, Intereconomics, 57(3), pp. 164–170.
17. UNICEF (2022) *UNICEF in Romania: Support for Refugee Children, Women and Families from Ukraine*. Available at: https://www.unicef.org/romania/stories/unicef-support-romania-refugee-children-women-and-families-coming-ukraine.
18. ACTED (2022) *Ukraine Conflict: How We Support Refugees in Moldova*. Available at: https://www.acted.org/en/ukraine-conflict-how-we-support-refugees-in-moldova/.
19. UNHCR (2025) *Ukraine Refugee Situation: Slovakia Refugee Data Portal*. Available at: https://data.unhcr.org/en/situations/ukraine/location/10785.
20. Statistics Poland and World Health Organization (2023) *Health of refugees from Ukraine in Poland 2022: Household survey and behavioural insights research*, Warsaw, Poland.
21. International Organization for Migration (2022) *Ukraine Response 2022 – Slovakia: Displacement patterns, needs and intentions survey*.
22. Suleimenova, D. and Groen, D. (2020) *How policy decisions affect refugee journeys in South Sudan: a study using automated ensemble simulations*, Journal of Artificial Societies and Social Simulation, 23(1), p. 1.
23. Suleimenova, D., Low, W. and Groen, D. (2022) *An agent-based forced displacement simulation: A case study of the Tigray crisis*, Lecture Notes in Computer Science, pp. 83–89. doi:10.1007/978-3-031-08760-8_7.

ICCS Camera Ready Version 2026
To cite this paper please use the final published version:
DOI: 10.1007/978-3-032-29915-4_4